Full Text View

Volume 29, Issue 3 (March 1999)

Journal of Physical Oceanography
Article: pp. 500–511 | Abstract | PDF (205K)

The Modification of Long Planetary Waves by Homogeneous Potential Vorticity Layers

Roland A. de Szoeke and Dudley B. Chelton

College of Oceanic and Atmospheric Sciences, Oregon State University, Corvallis, Oregon

(Manuscript received November 13, 1997, in final form April 20, 1998)

DOI: 10.1175/1520-0485(1999)029<0500:TMOLPW>2.0.CO;2

ABSTRACT

A mechanism by which long planetary waves in the ocean may propagate significantly faster than the classical long baroclinic Rossby waves is investigated. The mechanism depends on the poleward thickening of intermediate density layers and the concomitant thinning of near-surface and deep layers. These features of the mass distribution are associated with the well-known homogenization of potential vorticity in intermediate density layers and with significantly elevated meridional potential vorticity gradients near the surface and somewhat at depth. The mechanism is explored in a simple three-layer model, in which the middle layer has zero potential vorticity gradient and is sandwiched between a surface layer with large potential vorticity gradient and a bottom layer with modest potential vorticity gradient. The effective phase speed of the planetary waves is merely the sum of the phase speeds of virtual baroclinic Rossby waves propagating on the individual layer interfaces as though the other interface were not there and as though there were no mean vertical shear. The mechanism is also examined for a continuous model with zero potential vorticity gradient throughout the interior and large virtual potential vorticity gradients near the surface and bottom. Planetary waves in these models can propagate westward up to twice as fast as baroclinic Rossby waves would through an ocean with the same vertical stratification, but no mean vertical shear. This explanation of the Rossby wave speedup complements a recent detailed theoretical calculation of planetary-wave phase speeds based on geostrophic velocity profiles from archived hydrographic data.

1. Introduction

Evidence is mounting for the ubiquitous occurrence of large-scale low-frequency westward-propagatingbaroclinic

planetary waves in low to mid latitudes (Freeland et al. 1975; White 1977, 1985 and references therein; Kessler 1990; Périgaud and Delecluse 1992; van Woert and Price 1993; LeTraon and Minster 1993; Aoki et al. 1995; Chelton and Schlax 1996; Cippollini et al. 1997). Quantitative attempts to account for the propagation speed of these waves by simple baroclinic Rossby wave theory have had limited success. In the standard theory, which neglects the effects of a background mean velocity field, long first-mode baroclinic Rossby waves should propagate with speed $-\beta\lambda^2_1$, that is, westward (β is the meridional gradient of the Coriolis parameter and λ_1 is the first baroclinic Rossby radius of deformation). Emery et al. (1984), Houry et al. (1987), Picaut and Sombardier (1993), and Chelton et al. (1998) have published maps of the geographic distribution of λ_1. At low latitudes (but beyond 5° of the equator, say) this simple expression for propagation speed does quite well [though Kessler (1990) remarks that tropical planetary waves appear to propagate more slowly than the classical long-wave formula predicts]. In middle latitudes, however, observed propagation speeds appear to be significantly larger in magnitude (White 1977; Kessler 1990; LeTraon and Minster 1993; Aoki et al. 1995; Chelton and Schlax 1996). Killworth et al. (1997) showed that this disparity is much reduced by taking into account the vertical shear associated with the mean circulation. Using historical hydrographic data to obtain the required climatological average buoyancy-frequency profiles and geostrophic velocity shear, they diagnostically calculated zonal phase speeds from the linearized quasigeostrophic potential vorticity equation. They carried out this calculation globally, for every 1° × 1° square. Dewar (1998) has computed phase speeds of planetary wave modes modified by mean circulation and demonstrated faster propagation than the standard theory. He finds that this speedup is due to the interaction of the waves with the background potential vorticity field, as modified by the mean circulation and the vertical shear.

Notwithstanding the success of the Killworth et al. (1997) calculations, it is difficult to sort out what features in the mean circulation and stratification fields are responsible for the increase of phase speed. For this purpose we consider in this paper simple models of planetary waves that we believe explain the speedup mechanism in the Killworth et al. model with minimal complexity. The first model consists of three layers, each of constant density, with differing mean zonal flows in each layer (section 2). The vertical shear gives different potential vorticity gradients in the three layers. A situation of particular interest occurs when the middle layer has zero potential vorticity gradient (section 3). Extensive geographical regions over which potential vorticity is remarkably uniform on a range of potential density surfaces have been identified by Keffer (1985) for the global ocean basins and Talley (1988) for the North Pacific. A theoretical mechanism for the homogenization of potential vorticity by the closed wind-driven circulation was proposed by Rhines and Young (1982). The role of such homogenized potential vorticity layers in determining the vertical distribution of the Sverdrup transport was discussed by Luyten et al. (1983) and de Szoeke (1987). Evidently, the thicknesses of such density layers increase poleward to offset the increase of the Coriolis parameter f and keep the potential vorticity $f\partial\rho/\partial z$ constant in each layer (relative vorticity may be neglected), where ρ is density. This means that shallow density surfaces are squeezed toward the sea surface, creating near-surface layers in which the meridional potential vorticity gradient is very large. For the same reason, deeper layers are squeezed toward the bottom, though the proportionate effect is smaller, giving an elevated potential vorticity gradient near the bottom, as observed for instance by Talley (1988).

In a three-layer model with zero potential vorticity gradient in the middle layer, designed to represent these features, we show that the effective planetary-wave phase speed, relative to the vertically averaged mean flow, is the sum of the phase speeds of virtual Rossby waves on the two individual layer interfaces, calculated as though the other interface were not there (section 3). Speedup ratios up to 2 (relative to the standard, unsheared case) can be achieved with layer-depth and density-increment choices that are plausible representations of nature. This contrasts to the usual experience with two-layer reduced-gravity models of sheared mean flows that give large near-surface potential vorticity gradients. The net effect on the westward propagation of planetary waves is zero or slight since the vortex stretching contribution of a sloping layer interface to the potential vorticity is compensated by an opposing Doppler shift. This has been referred to as the “non-Doppler effect” (Held 1983; Chang and Philander 1989; Herrmann and Kraus 1989; Kessler 1990). The important point is that two-layer reduced-gravity models cannot reproduce the mechanism for Rossby wave speedup in the model considered here.

In section 4, we examine the three-layer results in terms of the diagnostic analysis used by Killworth et al. (1997) to calculate propagation speeds based on mean zonal velocity profiles derived from climatological-average hydrographic data. We show how their qualitative conclusion that speedups of first-mode planetary waves are due to the presence of second-mode baroclinic structure in the mean velocity profile is related to the homogeneous potential vorticity structure of the interior, with enhanced effective β near the surface boundary especially.

In section 5 we present a simple continuous model of planetary wave propagation in which the mean velocity profile is chosen so that there is no interior potential vorticity gradient. The wave propagation is determined by the boundary conditions, in particular by the slope of the mean isopycnals (proportional to vertical shear) as they intersect the surface and bottom boundaries. When these slopes are opposite and the isopycnal slope is larger in magnitude at the bottom than at the surface, considerable speedups are achieved, of the order of 2, compared to simple Rossby wave propagation through unsheared water.

2. The layered model

A schematic diagram of the three-layer model is shown in Fig. 1. The mean thicknesses of the layers are D_1, D_2, D_3; the densities are ρ_1, ρ_2, ρ_3; and the mean zonal velocities are u_1, u_2, u_3; f is Coriolis parameter at a central latitude, β is the meridional gradient of Coriolis parameter, g is acceleration due to gravity, and ρ_0 is a representative water density. In the following, reduced-gravity parameters will appear, defined by $g_n = g(\rho_{n+1} - \rho_n)/\rho_0$ for $n = 1, 2$. The slope of the shallow layer interface is

$$s_1 = fg^{-1}{}_1(u_1 - u_2), \quad (2.1a)$$

shown as though positive on Fig. 1 (i.e., shoaling to the north); the slope of the deeper interface is

$$s_2 = fg^{-1}{}_2(u_2 - u_3), \quad (2.1b)$$

shown as though negative on Fig. 1.

The linearized quasigeostrophic potential vorticity equations for the three layers are

$$(u_1 - c)f^2D_1^{-1}g_1^{-1}(P_2 - P_1) + q_{1y}P_1 = 0 \quad (2.2a)$$

$$(u_2 - c)f^2D_2^{-1}\{-g_1^{-1}(P_2 - P_1) + g_2^{-1}(P_3 - P_2)\} + q_{2y}P_2 = 0 \quad (2.2b)$$

$$-(u_3 - c)f^2D_3^{-1}g_2^{-1}(P_3 - P_2) + q_{3y}P_3 = 0 \quad (2.2c)$$

(Pedlosky 1987); $P_j\Phi(x - ct, y)$ is the long-wavelength (longer than the baroclinic Rossby radius), long-period pressure perturbation in layer j propagating at zonal phase speed c with space–time structure $\Phi(x - ct, y)$. The coefficients of the second terms in Eqs. (2.2) are the meridional potential vorticity gradients in the respective layers, defined by

$$q_{1y}/\beta = 1 - \beta^{-1}f^2D_1^{-1}g_1^{-1}(u_2 - u_1) = 1 + fs_1/\beta D_1 \quad (2.3a)$$

$$q_{2y}/\beta = 1 + \beta^{-1}f^2D_1^{-1}\{g_1^{-1}(u_2 - u_1) - g_2^{-1}(u_3 - u_2)\} = 1 - \beta^{-1}fD_2^{-1}(s_1 - s_2) \quad (2.3b)$$

$$q_{3y}/\beta = 1 + \beta^{-1}f^2D_3^{-1}q_2^{-1}(u_3 - u_2) = 1 - fs_2/\beta D_3. \quad (2.3c)$$

The schematic in Fig. 1 is motivated by meridional density sections like the one shown in Fig. 2 from the western Pacific. This figure shows near-surface isopycnals shoaling polewards at midlatitudes, overlying isopycnal layers thickening poleward in such a way that the product $f\partial\rho/\partial z$ remains constant. This is emphasized by the middepth cross-hatching in Fig. 2, which shows the latitudinal extent, at this longitude, of homogenized potential vorticity in density layers, as judged from Keffer's (1985) maps of this quantity. This figure also shows (in the lower panel) that in the deep North Pacific, below 3000 m and up to 45°N, isopycnals slope downward to the north.

Multiplying Eq. (2.2) by D_1, D_2, D_3 and adding, one obtains

$$\beta(D_1P_1 + D_2P_2 + D_3P_3) = 0. \quad (2.4)$$

This relation does not involve the zonal phase speed c. It means that the solutions of (2.2) have no barotropic component. (The barotropic mode, in the long-wave limit for a rigid lid as considered here, has infinite westward phase speed.)

By making the substitutions

$$P_1 = -\frac{W_1}{D_1}, \qquad P_2 = \frac{W_1 - W_2}{D_2}, \qquad P_3 = \frac{W_2}{D_3}, \quad (2.5)$$

an analog is obtained of Killworth et al.'s (1997) equation for vertical velocity in the continuous case. Equation (2.4) is automatically satisfied and the number of independent variables is reduced to two. The dimensional vertical velocities at the interfaces between the layers are given by $\beta(f^2\rho_0)^{-1}W_j\partial\Phi/\partial x$. Equations (2.2a) and (2.2c) become

$$-\left(\frac{u_1 + u_2}{2} - c\right)\left(\frac{W_1 - W_2}{D_2} + \frac{W_1}{D_1}\right)$$

$$-\frac{u_1 - u_2}{2}\left(\frac{W_1 - W_2}{D_2} + \frac{W_1}{D_1}\right) + \frac{\beta g_1}{f^2}W_1 = 0 \quad (2.6a)$$

$$-\left(\frac{u_2 + u_3}{2} - c\right)\left(\frac{W_2}{D_3} - \frac{W_1 - W_2}{D_2}\right)$$

$$-\frac{u_2 - u_3}{2}\left(\frac{W_2}{D_3} + \frac{W_1 - W_2}{D_2}\right) + \frac{\beta g_2}{f^2}W_2 = 0. \quad (2.6b)$$

Equation (2.2b) is the difference between these two equations.

a. Standard theory

Before examining the case of homogeneous potential vorticity in the middle layer, we shall consider the case of no background mean flow, $u_1 = u_2 = u_3 = 0$. We call this the standard theory. In this case, Eqs. (2.6) may be written

$$\frac{W_1}{W_2} = d_2^{-1}\{d_1^{-1} + d_2^{-1} + c_0/c\}^{-1} \quad (2.7a)$$

$$= d_2\{d_2^{-1} + d_3^{-1} + c_0/cr\}, \quad (2.7b)$$

where $d_i = D_i/H$ are the scaled mean layer thicknesses, $H = D_1 + D_2 + D_3$ being the total water depth,

$$r = \frac{\rho_2 - \rho_1}{\rho_3 - \rho_2} = \frac{g_1}{g_2} \quad (2.8)$$

is the ratio of the density differences (or reduced gravities) at the two layer interfaces, and $c_0 = \beta g_1 H/f^2$ is a Rossby wave propagation speed scale. The second equality of (2.7) gives a quadratic equation for c, whose solutions are

$$\frac{c_0}{c} = -\frac{1}{2}[d_1^{-1} + d_2^{-1} + r(d_2^{-1} + d_3^{-1})]$$

$$\pm \frac{1}{2}\{[d_1^{-1} + d_2^{-1} - r(d_2^{-1} + d_3^{-1})]^2 + 4rd_2^{-2}\}^{1/2}. \quad (2.9)$$

Both solutions for c are negative (i.e., westward). The larger in magnitude, given by the plus sign in (2.9), represents the first baroclinic Rossby wave mode; the other represents the second baroclinic mode.

For later reference, we rewrite the results of (2.9) in altered forms designed to bring out their relation to various two-layer systems and to introduce parameters that embody their symmetries and will become useful in the following sections. The two values of c given by (2.9) may be written as

$$c_i = -\beta\lambda^2{}_i, \qquad i = 1, 2, \tag{2.10}$$

where the λ_i are the baroclinic Rossby radii of deformation for the three-layer system. They can be written in either of the forms

$$\begin{aligned}\lambda_i^2 &= 2\lambda_1^{2*}\{p + 1 \pm [(p-1)^2 + 4p\delta]^{1/2}\}^{-1} \\ &= 2\lambda_2^{2*}\{p^{-1} + 1 \pm [(p^{-1}-1)^2 + 4p^{-1}\delta]^{1/2}\}^{-1}. \end{aligned} \tag{2.11}$$

In this formula

$$\lambda_1^{2*} = g_1 H f^{-2}(d_1^{-1} + d_2^{-1})^{-1}, \tag{2.12a}$$

$$\lambda_2^{2*} = g_2 H f^{-2}(d_2^{-1} + d_3^{-1})^{-1} \tag{2.12b}$$

are the Rossby radii in the two-layer systems consisting, respectively, of layers 1 and 2 only and layers 2 and 3 only. The parameter p is

$$p = r\frac{d_2^{-1} + d_3^{-1}}{d_1^{-1} + d_2^{-1}} = \frac{\lambda_1^{2*}}{\lambda_2^{2*}}, \tag{2.12c}$$

that is, the ratio of the Rossby wave phase speeds $-\beta\lambda^2{}_1{}^*$ and $-\beta\lambda^2{}_2{}^*$ in the virtual two-layer systems just mentioned. It may also be written as

$$p = r\frac{d_1(1-d_1)}{d_3(1-d_3)} = \frac{\tilde{c}_1}{\tilde{c}_2}, \tag{2.12d}$$

where $\tilde{c}_1$ and $\tilde{c}_2$ are the Rossby wave phase speeds in another pair of virtual two-layer systems obtained, respectively, by merging layers 2 and 3 (i.e., setting $\rho_2 = \rho_3$) and by merging layers 1 and 2 ($\rho_1 = \rho_2$):

$$\tilde{c}_1 = -\beta g_1 H f^{-2}[d_1^{-1} + (d_2 + d_3)^{-1}]^{-1}, \tag{2.13a}$$

$$\tilde{c}_2 = -\beta g_2 H f^{-2}[(d_1 + d_2)^{-1} + d_3^{-1}]^{-1}. \tag{2.13b}$$

The parameter δ is

$$\delta = \frac{d_1}{d_2 + d_3}\frac{d_3}{d_1 + d_2} = \frac{d_1 d_3}{(1-d_1)(1-d_3)}. \tag{2.14}$$

This is the product of the ratio of the surface layer thickness to the rest of the water column and the ratio of the bottom layer thickness to the rest. Parameter δ is a coupling coefficient between the layer interfaces in the following sense. In the limit as the thickness of either the top layer or the bottom layer vanishes, $\delta \to 0$, while $g_1 d_1$ (or $g_3 d_3$) remains finite (so that parameter p remains finite and nonzero), Eq. (2.11) gives $\lambda^2{}_1 = \lambda^2{}_1{}^*$ and $\lambda^2{}_2 = \lambda^2{}_2{}^*$ (assuming the former is larger). In this limit the phase speeds (2.10) of the two baroclinic modes are $-\beta\lambda^2{}_1{}^*$ and $-\beta\lambda^2{}_2{}^*$, as though the upper and lower thermocline were decoupled.

The parameters p and δ are written as functions of d_1, d_3, r. They exhibit the following symmetries:

$$\delta(d_3, d_1) = \delta(d_1, d_3). \qquad (2.15b)$$

These symmetries show that the disturbances in an ocean with the order of density jumps and layer thicknesses reversed propagate with identical phase speed.

b. Examples: Standard case

For three sets of choices of scaled depths d_1, d_2, d_3 and reduced-gravity ratio r, we have calculated the p and δ parameters, the first and second baroclinic Rossby radii of deformation, and the corresponding standard Rossby wave-mode phase speeds. These are shown in Table 1 and will be used later to contrast the effects of vertical shear on planetary-wave propagation speed. The most symmetric distribution of density, example (i), furnishes the fastest Rossby wave phase speeds. The more realistic distributions, examples (ii) and (iii), skewed toward the surface and with large density ratios, furnish slower phase speeds. Figure 3 shows the vertical profiles of the first (a) and second (b) pressure modes (in arbitrary units) for the three examples; it also shows the vertical velocity at the first interface, W_1, relative to W_2 at the second interface (assumed = 1). The first mode is always sinuous in its vertical structure; the second mode is varicose.

3. Middepth homogeneous potential vorticity

In midlatitudes, shallow and intermediate density layers exhibit remarkable homogenization of potential vorticity. In Fig. 2 the regions of homogenization identified from Keffer's (1985) map have been indicated by crosshatching. This motivates the choice of setting to zero the meridional potential vorticity gradient of the middle layer of the model in section 2; that is, $q_{2y} = 0$. [If, further, interface slopes have the sense shown in Fig. 1, then potential vorticity gradients in the top and bottom layers are the same so that the Charney–Stern necessary condition for baroclinic instability is not fulfilled (Pedlosky 1987); all disturbances are neutrally stable.] Equations (2.2) simplify considerably. In the first place, the coefficient in the second term in (2.2b) vanishes so that, excluding the possibility that $c = u_2$,

$$P_2 - P_1 = r(P_3 - P_2). \qquad (3.1)$$

Using (3.1) and (2.4) to eliminate in favor of P_3 in (2.2c), one obtains

$$\frac{c - u_3}{c_0} = -d_3 q_{3y} \beta^{-1} r^{-1} \{1 - d_3 + r d_1\}. \qquad (3.2)$$

[Parameter c_0 was defined above, after Eq. (2.18).]

The potential vorticity gradients (2.3) may be written as

$$\frac{q_{1y}}{\beta} = 1 + \frac{s_1'}{d_1}, \qquad (3.4a)$$

$$\frac{q_{2y}}{\beta} = 1 + \frac{s_2' - s_1'}{d_2}, \qquad (3.4b)$$

$$\frac{q_{3y}}{\beta} = 1 - \frac{s_2'}{d_3}, \qquad (3.4c)$$

where

$$s_1' = \frac{f s_1}{\beta H} = \frac{u_1 - u_2}{c_0}, \qquad (3.5a)$$

$$s_2' = \frac{f s_2}{\beta H} = r \frac{u_2 - u_3}{c_0} \qquad (3.5b)$$

are the scaled interface slopes. The condition that $q_{2y} = 0$ relates the two slopes by

$$s'_2 = s'_1 - d_2, \tag{3.6}$$

and the potential vorticity gradient in the third layer becomes

$$\frac{q_{3y}}{\beta} = \frac{1 - d_1 - s'_1}{d_3}. \tag{3.7}$$

Substituting this into (3.2), and using

$$u_3 = \bar{u} - c_0\{d_1 s'_1 + r^{-1}(1 - d_3)(s'_1 - d_2)\},$$

where $\bar{u} = d_1u_1 + d_2u_2 + d_3u_3$ is the mean barotropic velocity, one obtains

$$\frac{c - \bar{u}}{-c_0} = d_1(1 - d_1) + r^{-1}d_3(1 - d_3). \tag{3.8}$$

The interpretation of this result is strikingly simple. Using (3.3), Eq. (3.8) may be written

$$c - \bar{u} = -\frac{\beta}{f^2}\{g_1[D_1^{-1} + (D_2 + D_3)^{-1}]^{-1} + g_2[D_3^{-1} + (D_1 + D_2)^{-1}]^{-1}\}. \tag{3.9}$$

The right side is simply $\tilde{c}_1 + \tilde{c}_2$, given by (2.13). This is the sum of the phase speeds of long internal Rossby waves travelling on the respective interfaces *as though the other interface were not there* and as though there were no mean sheared motion. When $D_1 \ll D_2$, D_3 and $r \gg 1$, which resembles the typical oceanic situation, the phase speed c_1 in the standard case of no mean flow (i.e., for the same stratification but with no internal isopycnal slope) is rather close to $\tilde{c}_1$. Hence, the extra term in (3.8) or (3.9) represents a speedup of the standard case.

More precisely, $(c - \bar{u})/c_1$ can be written as a function of d_1, d_3, r [recall that c_1 is given by (2.10), (2.11)], which can be expressed in terms of the two parameters p, δ given by (2.12d), (2.14). The result is

$$\frac{c - \bar{u}}{c_1} = \frac{1}{2}(1 - \delta)^{-1}\{p + 1 - [p^2 - 2p(1 - 2\delta) + 1]^{1/2}\} \times (1 + p^{-1}) \equiv \Gamma(p, \delta). \tag{3.10}$$

[The positive branch of the square root in (3.10) should always be taken.] We shall call Γ the speedup ratio. It satisfies the symmetry relation

$$\Gamma(p^{-1}, \delta) = \Gamma(p, \delta). \tag{3.11}$$

The parameter p is the ratio $\tilde{c}_1/\tilde{c}_2$ of the speeds of undisturbed virtual Rossby waves on the upper- and lower-layer interfaces [Eq. (2.12d)].

The speedup ratio Γ is contoured as a function of p and δ in Fig. 4. For $\delta < 0.1$ and p in the range $0.5 < p < 2.0$, values of Γ greater than 1.5 can be obtained. The maximum value of Γ for fixed δ occurs at $p = 1$, when the undisturbed phase speeds on the individual interfaces are matched, so that $\Gamma = 2/(1 + \delta^{1/2})$, which approaches 2 for small δ. For $d_1 \ll d_3 \sim O(1)$, typical of the real ocean, the parameters given by (2.12d), (2.14) are approximately $p \approx rd_1/d_3(1 - d_3)$ and $\delta \approx$

$d_1 d_3/(1 - d_3) \ll 1$. Attaining a large speedup ratio Γ, approaching 2, in the real ocean requires a large density ratio $r \sim d_3(1 - d_3)/d_1$. Note that $\Gamma = 1$ at $p = 0$ and $p = \infty$. These special cases represent, respectively, the removal of the upper or lower interfaces by setting $\rho_1 = \rho_2$ or $\rho_2 = \rho_3$: in other words, a two-layer situation for which no speedup can be achieved.

The theoretical maximum speedup ratio of $\Gamma = 2$ can be qualitatively understood from (3.8). Clearly, $c - \bar{u}$ must be less than twice the largest of the two terms on the right side of (3.8). Furthermore, the phase speed c_1 of the first mode in the standard case can be no larger than the largest of these two terms. It follows that $c - \bar{u}$ must be less than $2c_1$. It should be stressed that this bound on the speedup has been established only for the present case of zero middle-layer potential vorticity. Killworth et al. (1997) report speedup ratios higher than 2, calculated both numerically and by approximate analytical methods. In the latter, arbitrary speedups can be accomplished by adding sufficient baroclinic mode-2 structure to the mean velocity profile (see section 4). Yet the global calculation of local phase speeds done by the Killworth et al. numerical methods furnishes very few instances of speedup ratios larger than 2 (Fig. 5).

Three examples of mean flow profiles are shown in panels (c) of Fig. 3. These are constructed to give zero flow in the third layer and scaled so that meridional potential vorticity gradient in the middle layer is zero. The resulting scaled interface slopes, (3.5a,b), are shown in Table 1. The potential vorticity gradients of layers 1 and 2 in example (i), the most symmetric, are only modestly elevated above β. The potential vorticity gradients of layer 1 in example (ii), and especially example (iii), are highly elevated over β. Table 1 shows the speedup ratio Γ for the three examples modified by the shear profiles of Fig. 3c and the shear-modified phase speed $c = \Gamma c_1$. For the symmetric example, (i), the modified pressure mode is identical with the standard first-mode pressure wavefunction. For the skewed density distributions, the modified wavefunctions differ from the standard first-mode wavefunction. A good measure of this is the interface displacement ratio W_1/W_2: this is exactly one for example (i), 0.911 for example (ii), and even smaller, 0.677, for example (iii). The speedup ratio increases successively in the three examples, from 1.33 to 1.46 to 1.66, principally because δ, largely reflecting the scaled upper-layer thickness d_1, successively decreases (0.25, 0.11, 0.042). The parameter p is fairly close to unity for all three examples.

4. The general case of vertical shear

The special case of solutions for a mean zonal velocity profile constrained so that the potential vorticity gradient vanishes in the middle layer was considered in section 3. The solutions for a general mean zonal velocity profile can readily be obtained for the three-layer model by solving (2.6). For larger numbers of layers, or for the continuous limit, this becomes a tractable numerical problem, although insight can become obscured by complexity. A useful diagnostic is obtained by multiplying (2.6a) by W_1, (2.6b) by W_2, and adding. A counterpart of this diagnostic is available for an arbitrary number of layers, or for the continuous case (Killworth et al. 1997). The result is

$$c = B + S + V, \tag{4.1a}$$

where

$$B = -c_0\{w_1^2 + r^{-1}w_2^2\}, \tag{4.1b}$$

$$S = u_1\frac{w_1^2}{d_1} + u_2\frac{(w_1 - w_2)^2}{d_2} + u_3\frac{w_2^2}{d_3}, \tag{4.1c}$$

$$V = (u_1 - u_2)w_1\left(\frac{w_1 - w_2}{d_2} - \frac{w_1}{d_1}\right) + (u_2 - u_3)w_2\left(\frac{w_1 - w_2}{d_2} + \frac{w_2}{d_3}\right), \tag{4.1d}$$

with $w_i = W_i/D^{1/2}$, where

These terms are called respectively the beta term, the steering term, and the internal vortex stretching term.

The combination $S + V$ can be written

$$S + V = u_1 w_1 \frac{w_1 - w_2}{d_2} + u_2 \left(\frac{w_1^2}{d_1} + \frac{w_2^2}{d_3} \right) - u_3 w_2 \frac{w_1 - w_2}{d_2}. \quad (4.2)$$

If the mean zonal velocity profile reflects the shape of a baroclinic mode, that is, u_i is proportional to P_i given by (2.5), then $S + V = 0$. Hence, any amount of mean velocity having the same vertical profile as a baroclinic mode does not alter that particular mode.

From calculated solutions of the continuous quasigeostrophic potential vorticity equation, Killworth et al. noticed that the first-mode vertical-velocity wave function $W(z)$, modified by mean shear, usually differed little from the standard first-mode wave-function $W^{(1)}(z)$. This suggests that a first-order approximation of (4.1) can be obtained by substituting $W^{(1)}{}_j$ for the first mode. Note that only the ratio $W^{(1)}{}_1/W^{(1)}{}_2$, given by Eq. (2.7), matters in the expression (4.1b) for B. Then

$$B = -\beta\lambda^2{}_1 = c_1, \quad (4.3)$$

where c_1 is the phase speed of the first mode for the standard theory. The most general mean flow that can be envisaged is

$$u_i = a^{(1)} P^{(1)}{}_i + a^{(2)} P^{(2)}{}_i + \bar{u}, \quad (4.4)$$

where the $P^{(k)}{}_i$ are obtained from $W^{(k)}{}_j$ by (2.5). (The only effect of the vertical mean $\bar{u}$ is to Doppler-shift c by the same amount.) As noted above, the first-mode part of (4.4) has no effect on (4.1). Only the second-mode part contributes to the shear flow alteration of the mode-1 propagation speed. This contribution may be readily calculated from (2.10), (2.11) (choosing the negative sign option), and (4.1). In Fig. 3 the first and second pressure modes in panels (a) and (b) for all three examples have been so scaled that, with the ratio $a^{(1)}/a^{(2)} = 1$, Eq. (4.4) gives zero velocity in layer 3, $u_3 = 0$.

Consider the examples shown in Fig. 3 and Table 1. For example (i), because the shear-modified wavefunction is identical to the standard first mode, the approximation described above gives an exact result. For example (ii), the disturbed wavefunction amplitudes P_i are not identical to the undisturbed $P^{(1)}{}_i$, though they are qualitatively similar. The standard displacement ratio $W^{(1)}{}_1/W^{(1)}{}_2 = 0.846$ is quite close to the mean-shear-modified value $W_1/W_2 = 0.911$. As a consequence, the approximate enhanced phase speed $B^{(1)} + S^{(1)} + V^{(1)} = -3.65$ cm s^{-1}, based on the latter, is very similar to the exact value $c = -3.59$ cm s^{-1}. For example (iii), even though the mean-shear-modified wave-mode amplitudes P_i are similar to the standard case, the enhancement of the approximate wave speed $B^{(1)} + S^{(1)} + V^{(1)}$ gives rather too large an estimate, -2.35 cm s^{-1}, than the true value, -2.02 cm s^{-1}. Close inspection shows that the modified vertical displacement ratio $W_1/W_2 = 0.677$ is quite different from the standard ratio $W^{(1)}{}_1/W^{(1)}{}_2 = 0.335$, on which the $B^{(1)} + S^{(1)} + V^{(1)}$ calculation is based.

5. A continuous model

In this section, we examine a simple model with continuous stratification and mean shear flow, the latter chosen so that the interior potential vorticity gradient is exactly zero. It is again shown that the phase speed of disturbances, relative to the barotropic mean flow, is significantly larger than the first-mode baroclinic phase speed in the standard model with the same stratification, but without a mean shear flow. Some qualitative links with the layered model of section 3 are described.

The special mean shear–stratification combination considered here is one of a wide class of combinations that can give q_y

= 0. Williams (1974) considered the subset of this class for the case $\beta = 0$, which he called the generalized Eady problem. Lindzen (1994) and Swanson and Pierrehumbert (1995) also considered examples of the generalized Eady problem for $\beta \neq 0$ and stability and shear profiles that give $q_y = 0$. These authors concerned themselves mainly with modification of the baroclinic instability mechanism by homogenized interior potential vorticity.

The continuous linearized quasigeostrophic potential vorticity equation for long waves is

$$(u - c)\left(\frac{f^2 P_z}{N^2}\right)_z + q_y P = 0, \qquad (5.1)$$

where

$$q_y = \beta - (f^2 u_z / N^2)_z. \qquad (5.2)$$

The boundary conditions are

$$(u - c)\frac{f P_z}{N^2} - \frac{f u_z}{N^2} P = 0 \quad \text{at } z = 0, -H. \qquad (5.3)$$

In the limit of small layer thickness, Eq. (2.2b) becomes (5.1). Similarly, Eqs. (2.2a) and (2.2c) resemble the two boundary conditions (5.3) in the limit $D_1, D_3 \rightarrow 0$. Bretherton (1966) showed that the boundary conditions (5.3) may be replaced by the simpler $P_z = 0$ at $z = 0, -H$ if the potential vorticity gradient is replaced by the form

$$q_y^{\text{eff}} = q_y - \left(\frac{f^2 u_z}{N^2}\right)_0 \delta(z - \eta) + \left(\frac{f^2 u_z}{N^2}\right)_{-H} \delta(z + H + \eta),$$

and the limit $\eta \rightarrow 0$ is taken; here q_y is the interior potential vorticity gradient given by (5.2). This interpretation shows that the coefficients of the delta functions are the effective mean potential vorticity gradients due to the intersection of mean isopycnals with the surface and bottom, respectively.

We shall solve the system (5.1)–(5.3) for

$$q_y = 0, \qquad (5.4a)$$

$$N = N_0 e^{\alpha z}, \qquad (5.4b)$$

that is, zero interior potential-vorticity gradient and an exponential buoyancy-frequency profile. This is similar to choosing the middle layer's potential vorticity gradient zero in section 3. To ensure $q_y = 0$, the mean isopycnal slope at any level, proportional to the mean velocity shear, must satisfy

$$\frac{f u_z}{N^2} = \frac{\beta z}{f} + s_1. \qquad (5.5)$$

The constant s_1 is the slope at which isopycnals intersect the surface. The isopycnal slopes at the surface and bottom, s_1 and $s_2 = s_1 - \beta H/f$, are the counterparts of the interface slopes s_1, s_2 in the three-layer model, which appear in q_{1y} and q_{3y} in Eqs. (2.3a) and (2.3b). The Charney–Stern criterion, a necessary condition forbaroclinic instability, requires that s_1 and s_2 have the same sign. The hydrographic section exhibited in Fig. 2 shows that in the western North Pacific between 10° and 45°N these parameters in fact have opposite signs.

On integrating (5.5),

(5.6)

where $u(-H)$ has been chosen to be zero and $\epsilon = e^{-\alpha H}$. The vertically averaged mean current is then

$$\bar{u} = H^{-1}\int_{-H}^{0} u(z)\,dz$$

$$= \frac{\beta N_0^2}{4\alpha^2 f^2}\{1 - (-\ln\epsilon)^{-1} + \epsilon^2[1 + (-\ln\epsilon)^{-1}]$$

$$- (1 - s_1')[1 - \epsilon^2(1 - 2\ln\epsilon)]\}, \qquad (5.7)$$

where $s_1' = s_1 f/\beta H$ [cf. (3.5a)]. The phase speed c to be obtained below will be expressed relative to $\bar{u}$ so that the choice of $u(-H)$ is immaterial.

The solution of (5.1), given (5.4), is particularly simple. It is

$$P = A_1 e^{2\alpha z} + A_2, \qquad (5.8)$$

where A_1 and A_2 are arbitrary constants. Substituting this into the boundary conditions (5.3) and eliminating A_1 and A_2, one obtains

$$c = (1 - s_1')\left\{u(0) - \frac{\beta N_0^2}{2\alpha^2 f^2} s_1'(1 - \epsilon^2)(-\ln\epsilon)\right\}.$$

Substituting for $u(0)$ from (5.6), this becomes, relative to $\bar{u}$ given by (5.7),

$$c - \bar{u} = -\frac{\beta N_0^2}{4\alpha^2 f^2}\{1 - (-\ln\epsilon)^{-1} + \epsilon^2[1 + (-\ln\epsilon)^{-1}]\}. \qquad (5.9)$$

In general, the set of eigensolutions of (5.1) is severely truncated when there is a background mean vertical shear of the zonal velocity (Killworth and Anderson 1977). The solution given by (5.8), (5.9) is the *only* baroclinic mode that exists for the circumstances under which (5.4) pertains.

a. Standard case

For comparison, the solution of (5.1)–(5.3) for $u(z) \equiv 0$, and $N(z) = N_0 e^{\alpha z}$, can be readily determined analytically (Killworth et al. 1997). It is given in terms of first-order oscillatory Bessel functions of an argument proportional to $e^{\alpha z}$ (Abramowitz and Stegun 1964). The boundary conditions (5.3) require these solutions to be discrete normal modes with dispersion relations given by

$$c_i = -\beta\frac{N_0^2}{\alpha^2 f^2 \mu_i^2(\epsilon)}, \qquad (5.10)$$

for $i = 1, 2, \cdots$. These are the phase speeds of the baroclinic Rossby-wave modes, possessing i half-cycles of oscillation between the surface and bottom. For the choice of $\alpha^{-1} = 0.294H$ for the e-folding scale of the buoyancy frequency profile, giving $\epsilon = 1/30$ (suggested by Garrett and Munk 1972), the first two modes have eigenvalues

$$\mu_1 = 2.971, \qquad \mu_2 = 6.272.$$

The ratio of (5.9) to c_1, given by (5.10), is

$$\Gamma = \frac{c - \bar{u}}{c_1}$$

$$= \frac{\mu_1^2(\epsilon)}{4}\{1 - (-\ln\epsilon)^{-1} + \epsilon^2[1 + (-\ln\epsilon)^{-1}]\}. \quad (5.11)$$

For $\epsilon = 1/30$ the numerical value of this ratio is $\Gamma = 1.56$.

A qualitative link between this continuous model and the three-layer model of section 3 may be made as follows. Identify $rd_3/d_1 = (g_1/d_1)(g_2/d_3)^{-1}$ in the three-layer model with the ratio $N^2_0/N^2(-H) = e^{2\alpha H}$ in the continuous model. Select $d_1 = 1/60$, $d_3 = 0.5$ for the layered model. (Notice that d_3 is not especially small.) For $e^{\alpha H} = \epsilon^{-1} = 30$, we should select $r = 30$, and hence $\delta = 0.034$, $p = 1.93$, from Eqs. (2.14) and (2.12e). From Fig. 2 or Eq. (3.10) we then obtain $\Gamma \approx 1.5$, which is fairly close to the value of 1.56 calculated from (5.11).

This continuous, though highly idealized, model of the vertical stratification and shear structure reinforces the conclusion of the three-layer model that homogeneous internal potential vorticity layers and the concomitant hyper-β layers near the surface and, to some extent, the bottom can cause a significant speedup of westward planetary waves.

b. Topography

If there is a meridional gradient of bottom topography, then the boundary condition (5.3) has an additional term $-s_T P$ on the left side (s_T is the bottom slope, reckoned negative if shoaling northward). The consequence of this extra term is that Eq. (5.9) for $c - \bar{u}$ acquires an additional contribution

$$\frac{s_1' s_T'}{1 - s_T'} \frac{\beta N_0^2}{4\alpha^2 f^2}(1 + 2\epsilon^2 \ln\epsilon - \epsilon^2),$$

where $s'_1 = fs_1/\beta H$ and $s'_T = fs_T/\beta H$. Hence, Eq. (5.11) must be replaced by

$$\Gamma = \frac{c - \bar{u}}{c_1}$$

$$= \frac{\mu_1^2}{4}\left(1 - (-\ln\epsilon)^{-1} + \epsilon^2 - \frac{s_1' s_T'}{1 - s_T'}(1 + 2\epsilon^2 \ln\epsilon - \epsilon^2)\right). \quad (5.12)$$

If topography shoals northward, that is, $s'_T < 0$, the extra term in (5.12) enhances the speedup of the baroclinic planetary waves; if topography deepens northward, the speedup is diminished.

6. Summary

A mechanism has been described whereby long planetary waves may attain westward propagation speeds significantly larger than long first-mode baroclinic Rossby waves propagating through a still ocean. The mechanism depends on taking account of the effect of mean vertical shear in the potential vorticity balance of the waves. The vertical shear is directly related, through geostrophy, to the internal topography of density surfaces. The configuration of density surfaces in the ocean is such as to produce vertical ranges of density in which mean potential vorticity is very nearly homogeneous over horizontal regions encompassing significant fractions of entire ocean basins (Keffer 1985; Talley 1988). The vertical spacing of density surfaces increases poleward to offset the increase of the Coriolis parameter. Near the surface and bottom, however, lighter and denser layers are squeezed between the expanding midrange density layers and the respective boundary to produce layers with enhanced meridional potential vorticity gradient. This enhancement may be quite large near the

surface (perhaps as much as ten times the planetary vorticity gradient, β), more modest at the bottom (perhaps twice β).

In the three-layer model, with zero potential vorticity gradient in the middle layer, the planetary-wave phase speed is the sum of the vertically averaged mean flow and the phase speeds of the long baroclinic Rossby waves that would ride on the individual layer interfaces as though the other interface were absent, and as though there were no mean shear. Theoretical speedup ratios (compared to classical baroclinic modes with no mean shear) up to a value of two are possible. For plausible choices of oceanic parameters, speedup ratios of 1.5 and larger are readily conceivable.

By contrast, two-layer reduced-gravity models with strong eastward shear, giving an enhanced meridional potential vorticity gradient in the surface layer, do not show such a speedup (Held 1983; Chang and Philander 1989; Herrmann and Kraus 1989; Kessler 1990). The tendency of the enhanced potential vorticity gradient to increase propagation speeds is offset by the Doppler shift of the eastward mean flow; this has been termed the “non-Doppler effect.” The essential ingredient of the three-layer model is the middepth layer of homogeneous potential vorticity, which leads to the serial addition of the interfacial Rossby wave phase speeds. Such a feature cannot be represented in a model with fewer than three layers.

As an alternative qualitative model, we examined a continuous model in which vertical stratification decreases exponentially with increasing depth, while isopycnal slope decreases linearly at such a rate that there is no internal meridional potential vorticity gradient; the potential vorticity gradient is concentrated in virtual layers at the surface and bottom boundaries. This idealized model again showed that significant speedups of planetary wave propagation were possible, relative to the corresponding standard model with identical internal stratification and zero internal isopycnal slopes. It was shown that parameters characterizing these virtual boundary layers can be identified with parameters of the finite surface and bottom layers of the three-layer model. When the parameters of the continuous and three-layer models were selected to be comparable, similar speedup ratios were obtained for the two models.

The results of this paper suggest that the speedup ratios calculated by Killworth et al. (1997) by including the effects of climatological-average vertical shear in the mean circulation on planetary wave propagation are at least partially a consequence of such homogeneous potential vorticity features as observed at middepths in the ocean by Keffer (1985) and Talley (1988). In support of this claim we show a histogram of the speedup ratio calculated from historical hydrographic data by Killworth et al.’s (1997) method for 1° × 1° squares over the global ocean (Fig. 5). The histogram is strongly peaked for ratios near 1.0, with significant occurrences of ratios near 1.5, declining to virtually no occurrences of speedup ratios higher than 2.0. The latter bound concurs well with the theoretical limit of 2 for the speedup ratio obtained in section 3.

Acknowledgments

This research was supported by the Jet Propulsion Laboratory under the TOPEX/Poseidon Announcement of Opportunity, Contract 958127, by National Aeronautics and Space Administration Grant NAGW-3051, and by National Science Foundation Grants 9319892, 9402891, and 9402856. We thank Alison Macdonald for preparing the hydrographic section shown in Fig. 2.

REFERENCES

Abramowitz, M., and I. A. Stegun, 1964: *Handbook of Mathematical Functions.* Appl. Math. Ser. No. 55, U.S. Natl. Bur. Standards, 1046 pp..

Aoki, S., S. Imawaki, and K. Ichikawa, 1995: Baroclinic disturbances propagating westward in the Kuroshio Extension region as seen by a satellite altimeter and radiometers. *J. Geophys. Res.*, **100,** 839–855..

Bretherton, F. P., 1966: Critical layer instability in baroclinic flows. *Quart. J. Roy. Meteor. Soc.*, **92,** 325–334..

Chang, P., and S. G. H. Philander, 1989: Rossby wave packets in baroclinic mean currents. *Deep-Sea Res.*, **36,** 17–37..

Chelton, D. B., and M. G. Schlax, 1996: Global observations of oceanic Rossby waves. *Science*, **272,** 234–238..

— ,R. A. de Szoeke, M. G. Schlax, K. El Naggar, and N. Siwertz, 1998: Geographical variability of the first baroclinic Rossby radius of deformation. *J. Phys. Oceanogr.*, **28,** 433–460.. Find this article online

Cipollini, P., D. Cromwell, M. S. Jones, G. D. Quartly, and P. G. Challenor, 1997: Concurrent altimeter and infrared observations of Rossby wave propagation near 34°N in the northeast Atlantic. *Geophys. Res. Lett.*, **24,** 889–892..

de Szoeke, R. A., 1987: On the wind-driven circulation of the South Pacific Ocean. *J. Phys. Oceanogr.*, **17,** 613–630.. Find this article

online

Dewar, W. K., 1998: On “too fast” baroclinic planetary waves in the general circulation. *J. Phys. Oceanogr.*, **28,** 1739–1758.. Find this article online

Emery, W. J., W. G. Lee, and L. Magaard, 1984: Geographic and seasonal distributions of Brunt–Väisälä frequency and Rossby radii in the North Pacific and North Atlantic. *J. Phys. Oceanogr.*, **14,** 294–317.. Find this article online

Freeland, H. J., P. B. Rhines, and T. Rossby, 1975: Statistical observations of the trajectories of neutrally buoyant floats in the North Atlantic. *J. Mar. Res.*, **33,** 383–404..

Garrett, C., and W. Munk, 1972: Space–time scales of internal waves. *Geophys. Fluid Dyn.*, **2,** 225–264..

Held, I. M., 1983: Stationary and quasi-stationary eddies in the extratropical atmosphere: Theory. *Large-Scale Dynamical Processes in the Atmosphere*, B. J. Hoskins and R. P. Pearce, Eds., Academic Press, 127–168..

Herrmann, P., and W. Krauss, 1989: Generation and propagation of annual Rossby waves in the North Atlantic. *J. Phys. Oceanogr.*, **19,** 727–744.. Find this article online

Houry, S., E. Dombrowsky, P. De Mey, and J.-F. Minster, 1987: Brunt–Väisälä frequency and Rossby radii in the South Atlantic. *J. Phys. Oceanogr.*, **17,** 1619–1626.. Find this article online

Keffer, T., 1985: The ventilation of the world’s oceans: Maps of the potential vorticity field. *J. Phys. Oceanogr.*, **15,** 509–523.. Find this article online

Kessler, W. S., 1990: Observations of long Rossby waves in the northern tropical Pacific. *J. Geophys. Res.*, **95,** 5183–5217..

Killworth, P. D., and D. L. T. Anderson, 1977: Meaningless modes? *Mode Hot-Line News* (unpublished manuscript), No. 72, 1,3–4..

— ,D. B. Chelton, and R. A. de Szoeke, 1997: The speed of observed and theoretical long extratropical planetary waves. *J. Phys. Oceanogr.*, **27,** 1946–1966.. Find this article online

Le Traon, P.-Y., and J.-F. Minster, 1993: Sea level variability and semiannual Rossby waves in the South Atlantic subtropical gyre. *J. Geophys. Res.*, **98,** 12 315–12 326..

Lindzen, R. S., 1994: The Eady problem for a basic state with zero PV gradient but $\beta \neq 0$. *J. Atmos. Sci.*, **51,** 3221–3226.. Find this article online

Luyten, J. R., J. Pedlosky, and H. Stommel, 1983: The ventilated thermocline. *J. Phys. Oceanogr.*, **13,** 293–309.. Find this article online

Pedlosky, J., 1987: *Geophysical Fluid Dynamics.* 2d ed. Springer-Verlag, 710 pp..

Périgaud, C., and P. Delecluse, 1992: Annual sea level variations in the southern tropical Indian Ocean from Geosat and shallow-water simulations. *J. Geophys. Res.*, **97,** 20 169–20 178..

Picaut, J., and L. Sombardier, 1993: Influence of density stratification and bottom depth on vertical mode structure functions in the tropical Pacific. *J. Geophys. Res.*, **98,** 14 727–14 737..

Rhines, P. B., and W. R. Young, 1982: A theory of wind-driven circulation. I. Mid-ocean gyres. *J. Mar. Res.*, **40** (Suppl.), 559–596..

Swanson, K. L., and R. T. Pierrehumbert, 1995: Potential vorticity homogenization and stationary waves. *J. Atmos. Sci.*, **52,** 990–994.. Find this article online

Talley, L. D., 1988: Potential vorticity distribution in the North Pacific. *J. Phys. Oceanogr.*, **18,** 89–106.. Find this article online

van Woert, M. L., and J. M. Price, 1993: Geosat and advanced very high resolution radiometer observations of oceanic planetary waves adjacent to the Hawaiian Islands. *J. Geophys. Res.*, **98,** 14 619–14 631..

White, W. B., 1977: Annual forcing of baroclinic long waves in the tropical North Pacific. *J. Phys. Oceanogr.*, **7,** 50–61.. Find this article online

— ,1985: The resonant response of interannual baroclinic Rossby waves to wind forcing in the eastern midlatitude North Pacific. *J. Phys. Oceanogr.*, **15,** 403–415.. Find this article online

Williams, G. P., 1974: Generalized Eady waves. *J. Fluid Mech.*, **62,** 643–655..

Tables

Table 1. For various settings of mean layer depths and reduced gravity ratio in the three-layer model, Rossby radii of deformation, and Rossby wave phase speeds for the first and second baroclinic modes are shown (standard case). For the corresponding case modified by mean flows giving zero potential vorticity gradient in the middle layer, scaled interface slopes, and the resulting planetary wave speedup ratio are shown. The approximate calculation of speedup based on the method of section 4 is shown.

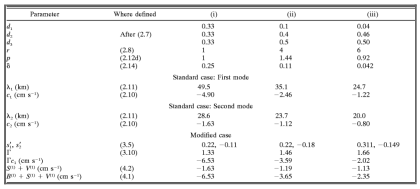

Parameter	Where defined	(i)	(ii)	(iii)
d_1		0.33	0.1	0.04
d_2	After (2.7)	0.33	0.4	0.46
d_3		0.33	0.5	0.50
r	(2.8)	1	4	6
p	(2.12d)	1	1.44	0.92
h	(2.14)	0.25	0.11	0.042
		Standard case: First mode		
λ_1 (km)	(2.11)	49.5	35.1	24.7
c_1 (cm s^{-1})	(2.10)	−4.90	−2.46	−1.22
		Standard case: Second mode		
λ_2 (km)	(2.11)	28.6	23.7	20.0
c_2 (cm s^{-1})	(2.10)	−1.63	−1.12	−0.80
		Modified case		
s_1', s_2'	(3.5)	0.22, −0.11	0.22, −0.18	0.311, −0.149
Γ	(3.10)	1.33	1.46	1.66
Γc_2 (cm s^{-1})		−6.53	−3.59	−2.02
$S^{(1)} + V^{(1)}$ (cm s^{-1})	(4.2)	−1.63	−1.19	−1.13
$\beta^{(1)} + S^{(1)} + V^{(1)}$ (cm s^{-1})	(4.1)	−6.53	−3.65	−2.35

Click on thumbnail for full-sized image.

Figures

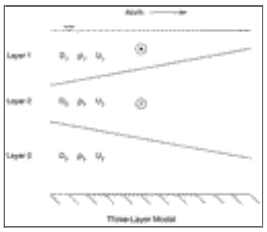

Click on thumbnail for full-sized image.

Fig. 1. Schematic of the three-layer model. The slopes of the interfaces are shown for eastward mean shear near the surface and westward mean shear at middepth.

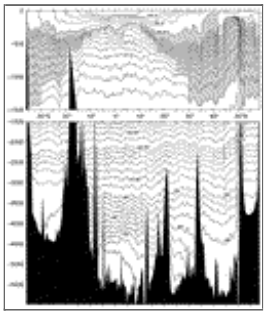

Click on thumbnail for full-sized image.

Fig. 2. Potential density (σ_θ referenced to 0 dbar above 1500 m, σ_4 referenced to 4000 dbar below 1500 m) along 179°E in the western Pacific. Note the northward–upward isopycnal slopes near surface; northward–downward slopes at middepth. The hatched region corresponds to the range over which Keffer's (1985) maps show potential vorticity approximately homogeneous on isopycnal surfaces.

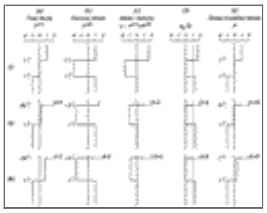

Click on thumbnail for full-sized image.

Fig. 3. Features of three example calculations with the three-layer model using the parameter settings in columns (i), (ii), and (iii) of Table 1. For the standard case (no shear) the first- (a) and second-mode (b) vertical profiles of pressure are shown (arbitrary units). The interfacial vertical velocities of the modes are indicated on these panels by arrows with accompanying numerical magnitudes, relative to $W_2 = 1$. (c) Mean velocity profiles constructed from first and second modes with zero mean and zero bottom velocity (unit: cm s^{-1}); and (d) associated meridional potential vorticity gradients (scaled by β). (e) The shear-modified pressure modes for (c) and (d) (arbitrary units); interfacial vertical velocities are indicated.

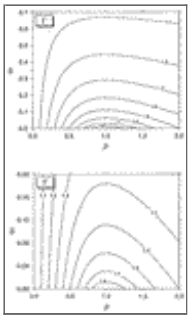

Click on thumbnail for full-sized image.

Fig. 4. The speedup ratio c/c_1 for zero interior potential vorticity gradient as a function of parameters p, δ, depending on density difference ratio r and mean layer depths D_1, D_2, D_3.

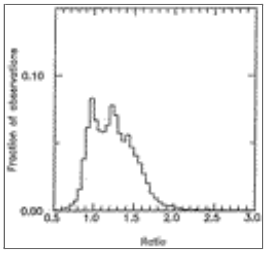

Click on thumbnail for full-sized image.

Fig. 5. A histogram of the ratio of planetary-wave phase speed calculated by the Killworth et al. (1997) method including mean vertical shear, to Rossby wave phase speed obtained by neglecting mean shear (Chelton et al. 1998) for 1° × 1° squares over all ocean basins, 10°–50°S, 10°–50°N.

Corresponding author address: Dr. Roland A. de Szoeke, College of Oceanic and Atmospheric Sciences, Oregon State University, 104 Ocean Admin. Bldg., Corvallis, OR 97331-5503.

E-mail: szoeke@oce.orst.edu

top